Section 1
PROGRESS IN LASER FUSION

1.A OMEGA Phase Conversion with Distributed Phase Plates

Introduction

An essential requirement for direct-drive laser fusion is the uniform irradiation of spherical targets that are located in the quasi far field of a laser system. Uniform absorption of laser light results in improved spherical convergence of the target during high-density compression. A major impediment to irradiation uniformity with high-power, solid-state laser systems is the presence of hot-spot structure, in each of the frequency-converted beams, at the target plane.[1]

The hot-spot intensity nonuniformities are caused by spatial variations in the near-field phase front of each laser beam. Although for many tabletop applications diffraction-limited laser performance can be obtained through static phase correction, adaptive optics, or phase conjugation, such approaches are either excessively expensive, difficult to implement, or not yet available for large-aperture, high-peak-power laser beams.

An alternative to phase correcting a wave front involves modifying the laser beam's coherence properties, thereby changing its focusing characteristics. The method of induced spatial incoherence[2] involves a reduction in both spatial and temporal coherence. This technique currently precludes third-harmonic generation and requires expensive apparatus. Other methods are based on modifications of only the spatial coherence of a laser beam.[3,4] In general, a beam is subdivided into many beamlets, each individually phase modified (converted), and

then recombined at the target plane, much like a multibeam far-field interferometer.

A phase-conversion technology that incorporates a distribution of near-field phases to either perform static phase correction or induce spatial incoherence offers a degree of flexibility needed at this stage of research. Distributed-phase-plate technology, recently deployed on the OMEGA laser system, offers this parallel route toward increasingly higher levels of irradiation uniformity.

Analytical Design

Classical physical optics provides an understanding of the far-field intensity control obtained through phase conversion. A distributed phase plate (DPP), schematically represented in Fig. 33.1, is composed of an ordered array of transparent hexagonal elements. Phase retardation is randomly distributed among the elements by introducing optical path differences (OPD) using a thin-film layer of thickness t and refractive index n_λ. The exact amount

$$\phi = \frac{2\pi}{\lambda}\,[\mathrm{OPD}] = \frac{2\pi}{\lambda}\,[t\,(n_\lambda - 1)] \qquad (1)$$

of phase retardation ϕ experienced by a transmitted wave front depends upon the wavelength λ of light.

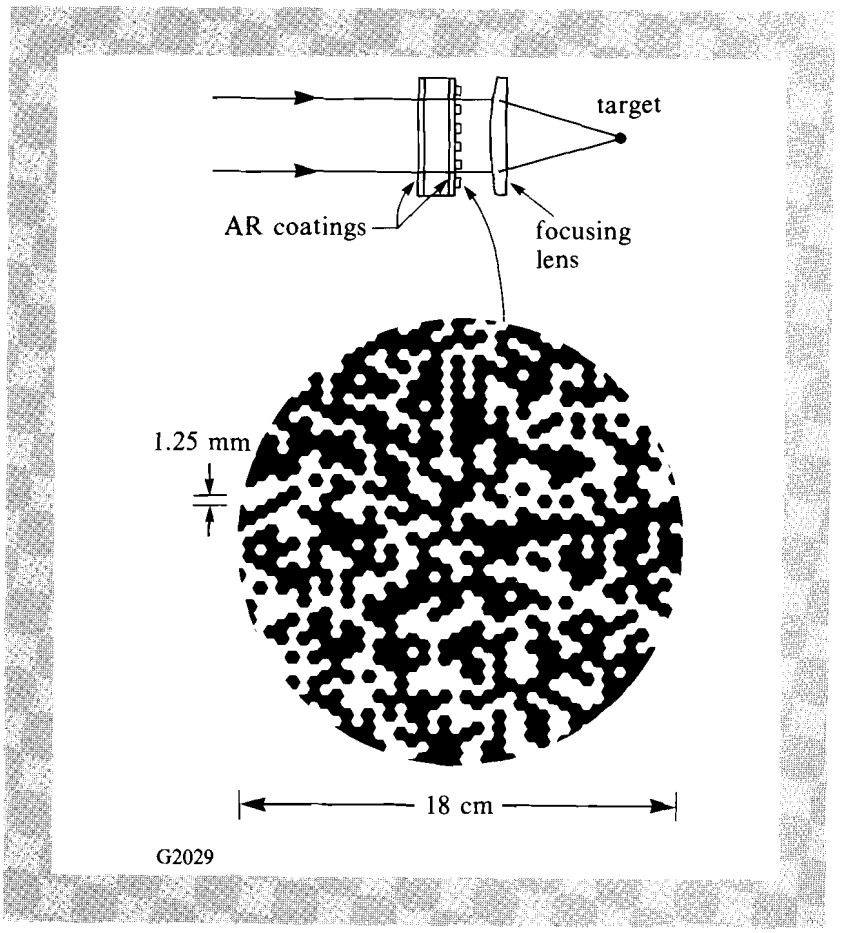

Fig. 33.1
Current distributed phase plates are composed of an ordered array of transparent elements. The phase values of approximately 15,000 hexagons are randomly binned into two levels that differ in phase by π radians. The diffraction patterns of the hexagonal beamlets are collected and brought to focus for target irradiation.

Collimated laser light is transmitted through the DPP, broken into coherent, phase-retarded beamlets, and brought to focus, where a superposition of beamlets is formed.[5] The amplitude distribution at the Fourier transform (focal) plane is given by

$$A\ (\epsilon,\eta) = \int_{-\infty}^{\infty}\int a\ (\alpha_1,\beta_1)\ e^{-2\pi i(\alpha_1\epsilon+\beta_1\eta)}\ d\alpha_1\ d\beta_1\ , \qquad (2)$$

where $a(\alpha_1, \beta_1)$ is the complex amplitude distribution and $\epsilon = \alpha_2/(\lambda f)$, $\eta = \beta_2/(\lambda f)$ are the spatial-frequency variables. The input amplitude is a product of the laser beam amplitude (denoted by the subscript L) and the amplitude transmittance of the DPP:

$$a\ (\alpha_1,\ \beta_1) = \Psi_L\ (\alpha_1,\ \beta_1) e^{i\phi_L\ (\alpha_1,\beta_1)} \cdot \sum_{j=1}^{N}\sum_{k=1}^{N} \mathrm{CIRC}\left[\frac{\sqrt{(\alpha_1-\alpha_j)^2 + (\beta_1-\beta_k)^2}}{d_o}\right] e^{i\phi_{R_{j,k}}}\ . \qquad (3)$$

The circle function (CIRC)[6], defined as

$$\mathrm{CIRC}\left[\frac{r}{d_o}\right] \equiv \begin{cases} 1 & o \le r < d_o/2 \\ 1/2 & r = d_o/2 \\ 0 & r > d_o/2 \end{cases} ,$$

closely approximates the hexagonal element. The random variable $\phi_{R_{j,k}}$ represents the phase retardation of the $(j,k)^{\text{th}}$ element. Substituting Eq. (3) into Eq. (2) yields

$$A\ (\epsilon,\eta) = \int_{-\infty}^{\infty}\int \Psi_L\ (\alpha_1,\ \beta_1)\ e^{i\phi_L\ (\alpha_1,\beta_1)} \sum_{j=1}^{N}\sum_{k=1}^{N} \mathrm{CIRC}\left[\frac{\sqrt{(\alpha_1-\alpha_j)^2 + (\beta_1-\beta_k)^2}}{d_o}\right] e^{i\phi_{R_{j,k}}}\ e^{-2\pi i(\alpha_1\epsilon+\beta_1\eta)}\ d\alpha_1\ d\beta_1\ . \qquad (4)$$

Since the transform of a product is equal to the convolution of the individual transforms, $A(\epsilon, \eta)$ can be more conveniently expressed as

$$A\ (\epsilon,\ \eta) \propto A_L\ (\epsilon,\ \eta) \otimes \left[\frac{2\ J_1(\pi d_o\omega)}{\pi d_o\omega} \sum_{j=1}^{N}\sum_{k=1}^{N} e^{2\pi i\left(\epsilon\alpha_j+\eta\beta_k+\frac{\phi_{R_{j,k}}}{2\pi}\right)}\right]. \qquad (5)$$

The above expression represents the convolution (denoted by $\otimes$) between the far-field amplitude distribution of the laser beam $A_L(\epsilon, \eta)$ and the product of a low-frequency envelope and a superposition of random spatial-frequency harmonics. This convolution is responsible for the detailed power spectrum of the resulting intensity distribution. The envelope, known as the Besinc function, where

$$\omega = \sqrt{\epsilon^2 + \eta^2}\ ,$$

represents the slowly varying profile of the focal intensity distribution $I(\epsilon, \eta)$:

$$I(\epsilon, \eta) = A(\epsilon, \eta)\, A^*(\epsilon, \eta) \propto \left[\frac{2J_1(\pi d_0 \omega)}{\pi d_0 \omega}\right]^2 \tag{6}$$

The shape of this function, the Airy pattern, is shown in Fig. 33.2(a).

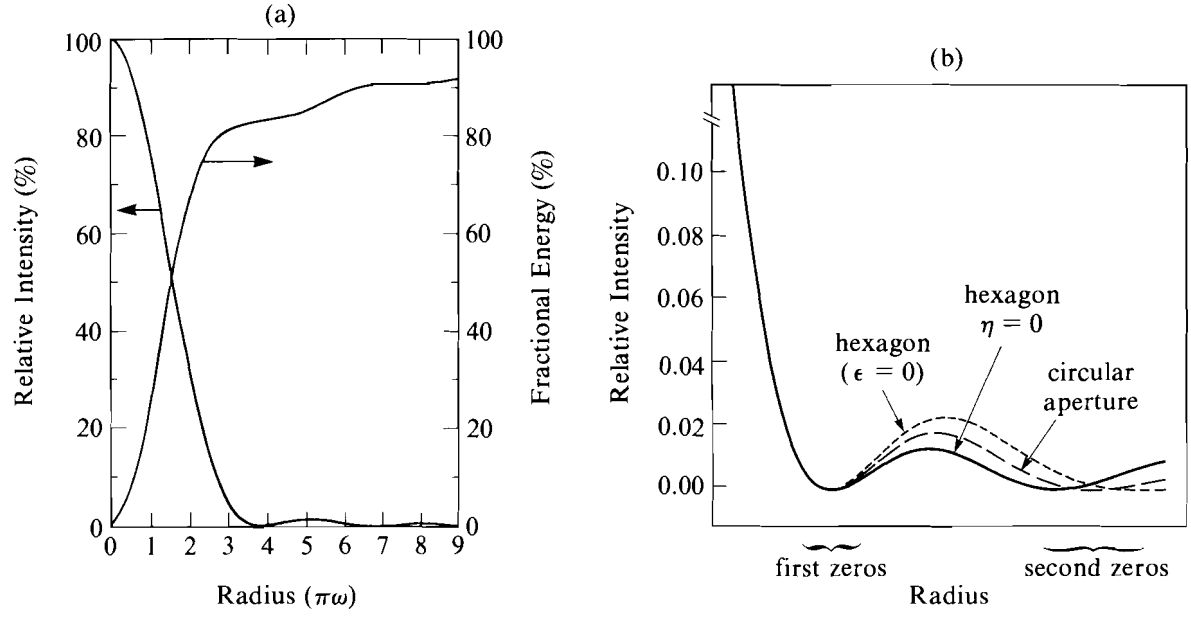

Fig. 33.2
(a) The encircled energy curve shows that more than 80% phase-conversion efficiency is obtained when the 5% intensity contour is tangentially mapped to the target. (b) The point-spread function (PSF) approximates the diffracted laser light, due to each hexagonal element, observed at the focal plane of a lens. The coherent addition of all the diffracted beamlets is also represented by a PSF envelope.

Since the actual diffraction structure is hexagonal and not circular, some justification for use of a circular aperture with an equivalent area is needed. Two major axes, along the lines of symmetry, define the profile of the hexagon Fourier transform. The transforms are given by

$$I(\epsilon, o) \propto \left[2\,\mathrm{sinc}(d\epsilon) + \mathrm{sinc}^2\left(\frac{d\epsilon}{2}\right)\right]^2 \tag{7}$$

and

$$I(o,\eta) \propto \left[4\,\mathrm{sinc}^2\left(\frac{d}{\sqrt{3}}\eta\right) - \mathrm{sinc}^2\left(\frac{d}{2\sqrt{3}}\eta\right)\right]^2, \tag{8}$$

where d is the hexagon width and $\mathrm{sinc}(x) \equiv \sin(\pi x)/(\pi x)$. Assuming equal areas, d and d_0 are related by $d_0 = (2\sqrt{3}/\pi)^{1/2}\, d$. Identical profiles, up to the first zero [as shown in Fig. 33.2(b)], validate modeling with a circular diffraction source of equivalent area.

From Eq. (6), and substitution of the spatial-frequency variable, the diameter of the first intensity zero is given by

$$D_{\mathrm{Airy}} = \frac{2.44\,\lambda f}{\left(\frac{2\sqrt{3}}{\pi}\right)^{1/2} d}, \tag{9}$$

where f is the lens focal length and λ is the wavelength of light. Equations (6) and (9) are used to design the DPP for a given target size and irradiation strategy. For the OMEGA laser, $\lambda = 0.351$ μm, $f = 593$ mm, and the target diameter is $D_T = 300$ μm. To obtain focusing with the 5.5% intensity contour at tangential focus, $D_{\text{Airy}} = 387$ μm, $d_o = 1.313$ mm, and $d = 1.250$ mm.

A simple relation determines the approximate number of hexagonal elements (N^2):

$$\left(\frac{D_{\text{Airy}}}{d_T}\right)^2 \sim \left(\frac{D_B}{d_o}\right)^2 = N^2 \sim 10{,}000 \ . \tag{10}$$

D_B is the beam diameter and d_T, the smallest intensity structure within the envelope, is approximately 1% of the target diameter.

The encircled fraction of energy[7] is given by

$$E_{\text{enc}}(\omega) = 1 - J_0^2(\pi d_o \omega) - J_1^2(\pi d_o \omega) \tag{11}$$

and is shown in Fig. 33.2(a). Table 33.I, showing the relative intensity and encircled energy as a function of target diameter, was generated from the plots in Fig. 33.2(a).

Table 33.I
Relative edge intensity and encircled energy versus target diameter.

Target Diameter (μm)	I/I_o(%)	E_{enc}(%)
280	9.1	79.5
290	7.2	80.6
300	5.5	81.5
310	4.2	82.2
320	2.9	82.8
387	0.0	83.8

G2232

DPP Fabrication and Testing

The fabrication procedure begins with the computer generation of an image containing a black-and-white version of the desired geometrical array of phase elements. Next, the fused-silica substrate is coated with antireflection coatings. The binary mask is transferred to the DPP glass substrate using photolithography. A positive photoresist layer is then spin deposited on one side of the substrate. After the resist layer is made more durable, through oven baking, it is exposed to ultraviolet radiation through the photographic mask. Chemical development of the photoresist produces a positive image of the photographic mask. A thorough cleaning process prepares the resist-mask substrate for the overcoat-deposition stage.

Following the production of the resist mask, a thin SiO_2 layer is vapor deposited over the same surface of the substrate. A subsequent

lift-off procedure removes the underlying resist, along with the SiO_2 overcoat that is in contact with the resist. The SiO_2 and antireflection interfaces remain intact, with a measured edge profile of <5-μm rms variation. These remaining SiO_2 hexagonal structures are the source of the π phase retardation.

As shown in Fig. 33.3, spectral measurement of the coating, before and after the overcoat deposition, is a sensitive method for measuring overcoat thickness. A 1% thickness reproducibility is routinely achieved. The OPD experienced by a transmitted wave front, however, is also dependent upon the refractive index [see Eq. (1)]. High-resolution interferometry has shown optical path variations, between plates, of about 1% to 2% of a $\lambda/2$ phase structure. Variations in the refractive index of the SiO_2 layer may account for this plate-to-plate OPD variability.

The phase retardation between two different levels on a DPP is accurately measured with laser interferometry. The DPP is inserted into one arm of a Twyman-Green interferometer, operating at the relevant wavelength of $\lambda = 0.351$ μm. Double-pass interference fringes are imaged onto a solid-state camera and the image captured with a frame grabber interfaced to an IBM PC-XT[8] computer. Image transfer to a SUN-3[9] provides the required complex Fourier transform capabilities to complete one-dimensional, spatial-synchronous phase detection (SSPD).[10] SSPD is performed, column by column, through the interface between the two elements of different phase. The calculated phase, averaged over a column, is plotted as a function of the column number. Since double-pass interferometry causes a $\lambda/2$ piston shift to appear as a wavelength shift, exactly one fringe shift indicates no phase error. A nearly perfect $\lambda/2$ piston shift is shown in Fig. 33.4. SSPD accuracy for piston measurement is approximately $\lambda/400$ for data of this quality. Fabrication accuracy of better than $\lambda/100$ has been demonstrated for the DPP's deployed on the OMEGA laser system.

OMEGA Implementation

The distributed phase plates are characterized off line with continuous-wave radiation of wavelength $\lambda = 0.351$ μm. In addition to phase measurement, plate transmission and far-field performance are both analyzed. DPP transmission typically results in $80\% \pm 1\%$ of the incident light reaching a 300-μm-diameter target placed at the focal plane. The intensity distribution exhibits the Airy pattern envelope and the high-modulation, high-frequency intensity variations, as predicted by the theoretical design of the DPP's. In addition, the overall focal distribution is found to be relatively insensitive to near-field phase and amplitude errors caused by, for example, atmospheric turbulence and beam obstructions.

Within the inner sleeves of each of the 24 focusing assemblies, ring adapters securely hold DPP's close to the focus lenses. This configuration provides several advantageous design features. Removal and reinsertion of all DPP's can be completed within a system shot cycle to accommodate optimum pointing of beams on target. In

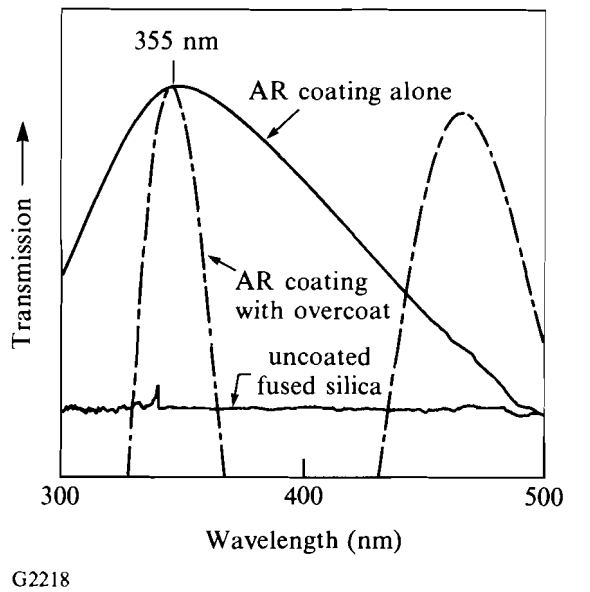

Fig. 33.3
The thin-film relief pattern is deposited over an antireflection coating. Spectral measurement of the coating, with and without an SiO_2 overcoat, is a sensitive method for determining the overcoat thickness. Optical path reproducibility of a few percent is limited by variations in the refractive index of SiO_2.

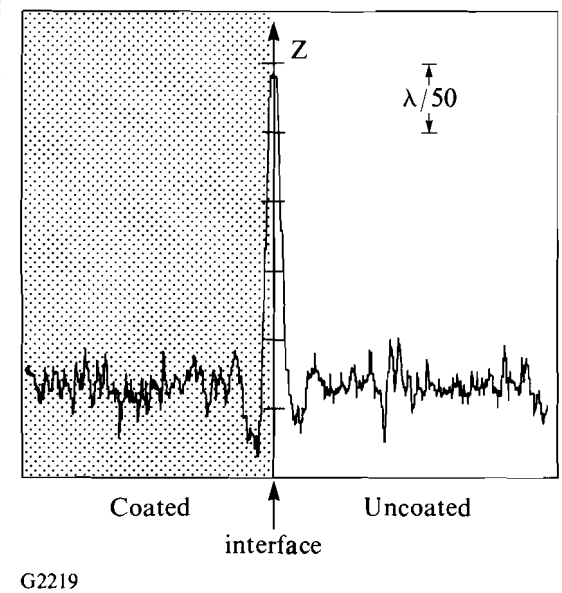

Fig. 33.4
The phase-retardance or optical-path difference between the two levels is accurately measured with laser interferometry. Spatial-synchronous phase detection is used to demonstrate better than λ/100 accuracy for a λ/2 hexagonal diffraction structure.

addition, the location near to the input side of the focus lens is relatively free of ghost radiation. Thin-film coating damage has not been observed. The OMEGA laser, barring laser component damage, can be operated at a fill factor that would normally degrade the uniformity on target. Therefore, the OMEGA laser system can be operated at higher uniformity and energy levels than were previously possible.

Equivalent-target-plane (ETP) intensity distributions are measured for beamline 6-2 of the OMEGA laser. Figure 33.5 shows the results for an ETP corresponding to a 300-μm-diameter target. DPP's provide a well-defined envelope, together with a power spectrum that is shifted to high spatial frequencies. Hot spots—of about 5%–10% of the target diameter—that are caused by near-field phase errors are replaced with fine speckle of about 1%–2% of the target diameter. Figure 33.6 quantifies the size and intensity of the hot spots and speckle.

Overall irradiation uniformity on target is assessed by computing a 24-beam superposition of intensities, followed by a spherical harmonic decomposition. Figure 33.7 compares the results for a typical OMEGA beamline, non-phase converted and phase converted. The rms (%) intensity nonuniformity is improved by a factor of 6 for modes $\ell = 2$

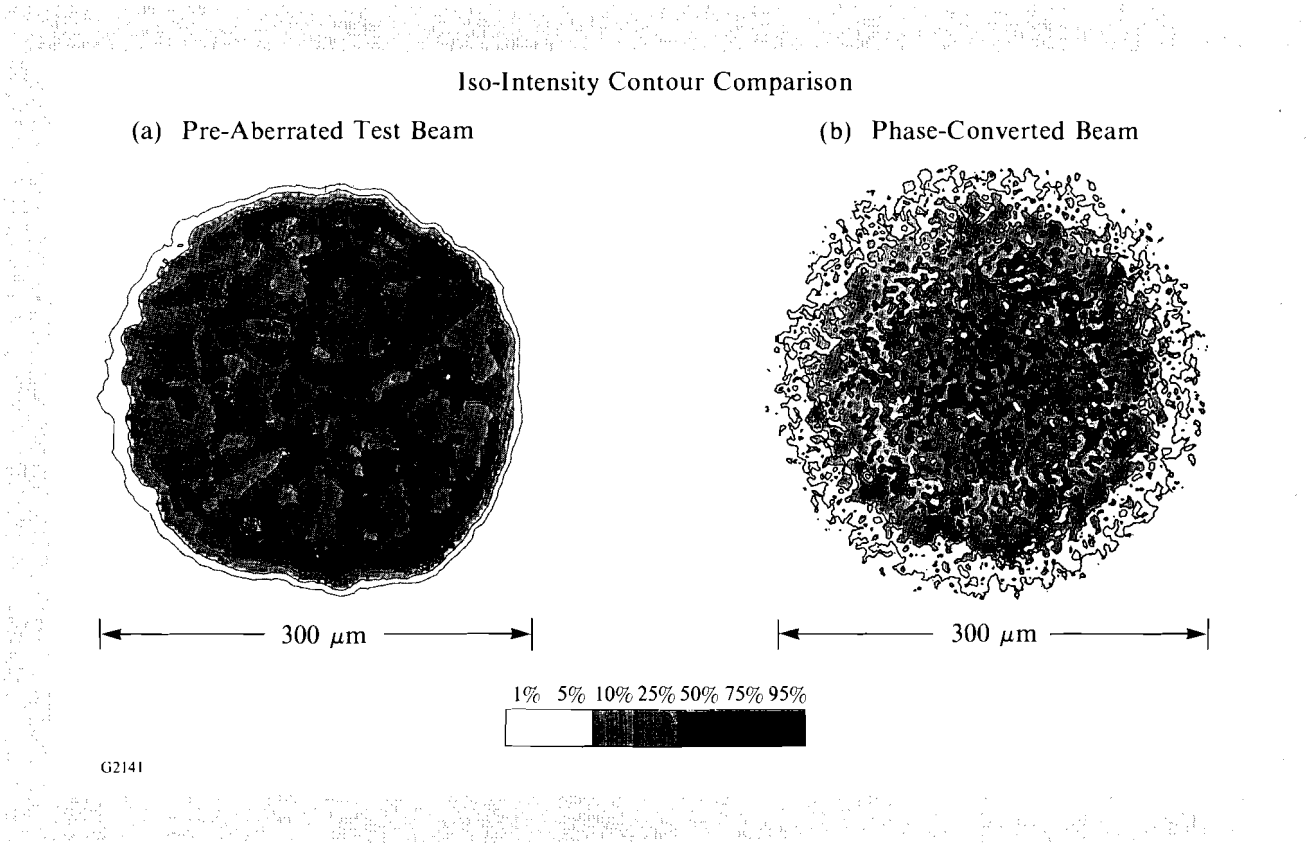

Fig. 33.5
Beamline 6-2 of the 24-beam OMEGA laser system is measured, before (a) and after (b) phase conversion, at an equivalent target plane of 300-μm diameter. Hot spots, caused by near-field phase errors, limit the uniformity levels on target. Distributed phase conversion produces a substantially different spatial-frequency spectrum, which is relatively insensitive to near-field phase errors.

through 20, and by a factor of 4 for modes $\ell = 2$ through 60. A smoothing of the beam by 1% of its diameter is assumed for this comparison.

A significant benefit of the DPP's is that they provide reproducible irradiation uniformity, which eliminates a major source of experimental compromise. Such reproducibility can be obtained with the OMEGA laser without DPP's only if atmospheric turbulence, beam misalignment, and accumulated birefringence are substantially reduced.

Applications

An essential requirement of direct-drive, inertial confinement fusion is the uniform irradiation of spherical targets that are placed in the quasi far field of a laser beam. Distributed phase plates provide substantially improved uniformity levels for targets placed close to the far-field plane. In addition to this primary goal, a variety of applications exists for this class of optical elements. As an example, the cylindrical focusing of laser light for x-ray laser target irradiation could include a DPP, since the narrow dimension of such targets is generally one to two orders of magnitude greater than the diffraction limit.

Further progress in distributed phase technology is anticipated. Higher levels of uniformity are expected with either N-level ($N \geq 3$) phase plates[11,12] or plate geometries that produce supergaussian

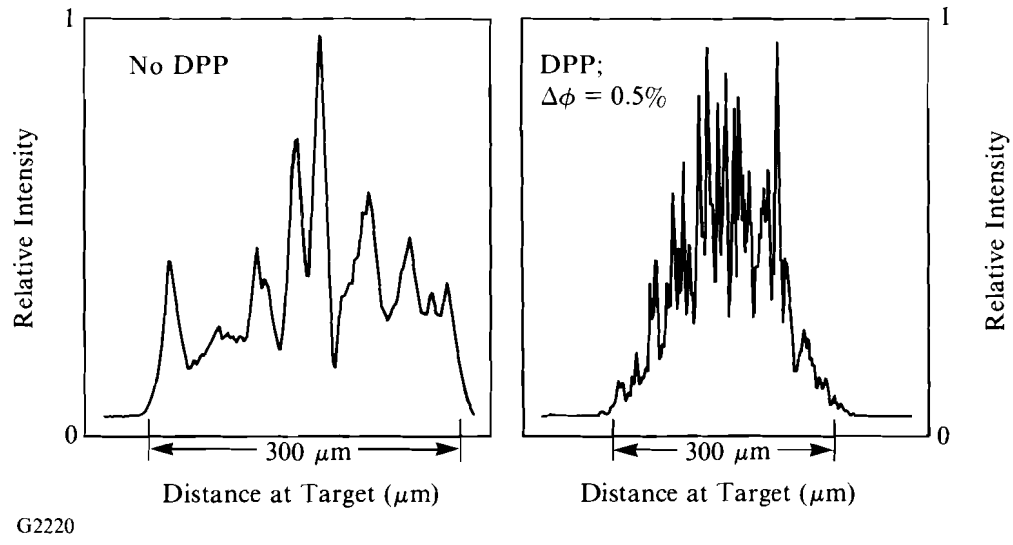

Fig. 33.6
Cross sections of the target-plane intensity distributions in Fig. 33.5 show, quantitatively, the differences before and after phase conversion. Numerous hot spots, each about 5%–10% of the target-plane beam diameter, are replaced by a reproducible and uniform envelope that contains small-scale speckle.

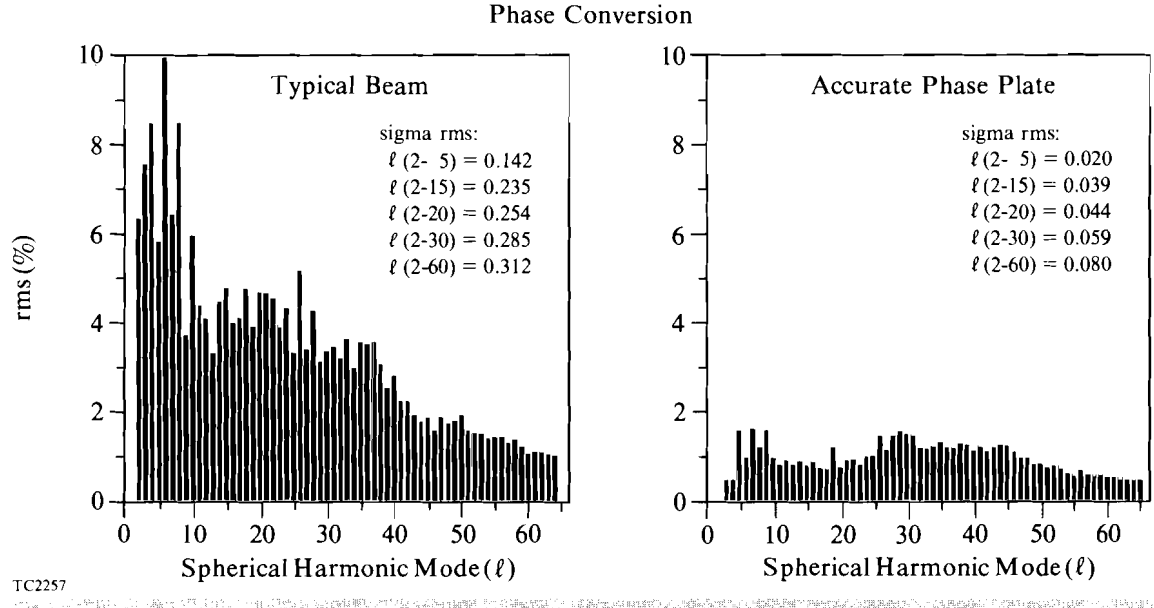

Fig. 33.7
Overall improvement of the irradiation uniformity on target is assessed by computing a 24-beam superposition of intensities and a spherical harmonic decomposition. The rms (%) intensity nonuniformity is improved by a factor of 6 for modes ℓ = 2 through 20, and by a factor of 4 for modes ℓ = 2 through 60. Smoothing by 1% of the beam diameter is assumed.

intensity profiles. Multiwavelength devices are also feasible. Furthermore, the DPP technology is a candidate for high-damage-threshold diffraction gratings.

Conclusion

The joining of many diverse technologies has resulted in the design, fabrication, and testing of high-quality distributed phase plates. Computerized image generation, photolithography, chemical vapor deposition, and high-resolution interferometry have been combined to make OMEGA the only frequency-tripled and phase-converted laser system. DPP's have improved the irradiation uniformity at the target plane by more than a factor of 3. In addition, the increased reproducibility of the beam profiles offered by the DPP's has made possible more critical assessment of shot-to-shot variations in beam energy balance and beam pointing. Other applications for distributed phase technology are anticipated.

ACKNOWLEDGMENT

This work was supported by the U.S. Department of Energy Office of Inertial Fusion under agreement No. DE-FC08-85DP40200.

REFERENCES

1. S. Skupsky and T. Kessler, *Phys. Rev.* (submitted for publication).
2. R. H. Lehmberg, A. J. Schmitt, and S. E. Bodner, *J. Appl. Phys.* **62**, 2680 (1987).
3. X. Deng *et al.*, *Appl. Opt.* **25**, 377 (1986).
4. Y. Kato *et al.*, *Phys. Rev. Lett.* **53**, 1057 (1984).
5. C. B. Burckhardt, *Appl. Opt.* **9**, 695 (1970).
6. J. D. Gaskill, *Linear Systems, Fourier Transforms, and Optics* (Wiley, New York, 1987), pp. 66–77.
7. M. Born and E. Wolf, *Principles of Optics*, 6th corrected ed. (Pergamon Press, New York, 1980), pp. 395–398.
8. PC-XT is a trademark of IBM, P.O. Box 1328-S, Boca Raton, FL 33432.
9. SUN is a trademark of SUN Microsystems, Inc., 2550 Garcia Avenue, Mountain View, CA 94043.
10. LLE Review **31**, 114 (1987).
11. W. C. Stewart, A. H. Firester, and E. C. Fox, *Appl. Opt.* **1**, 604 (1972).
12. Y. Takeda, Y. Oshida, and Y. Miyamura, *Appl. Opt.* **11**, 818 (1972).